nature neuroscience

Non-invasive mapping of connections between human thalamus and cortex using diffusion imaging

T E J Behrens[1,2,4], H Johansen-Berg[1,4], M W Woolrich[1,2], S M Smith[1], C A M Wheeler-Kingshott[3], P A Boulby[3], G J Barker[3], E L Sillery[1], K Sheehan[1], O Ciccarelli[3], A J Thompson[3], J M Brady[2] & P M Matthews[1]

Evidence concerning anatomical connectivities in the human brain is sparse and based largely on limited post-mortem observations. Diffusion tensor imaging has previously been used to define large white-matter tracts in the living human brain, but this technique has had limited success in tracing pathways into gray matter. Here we identified specific connections between human thalamus and cortex using a novel probabilistic tractography algorithm with diffusion imaging data. Classification of thalamic gray matter based on cortical connectivity patterns revealed distinct subregions whose locations correspond to nuclei described previously in histological studies. The connections that we found between thalamus and cortex were similar to those reported for non-human primates and were reproducible between individuals. Our results provide the first quantitative demonstration of reliable inference of anatomical connectivity between human gray matter structures using diffusion data and the first connectivity-based segmentation of gray matter.

The anatomical connectivity pattern of a brain region determines its function[1]. Although invasive tracer studies have produced a large body of evidence concerning connectivity patterns in non-human animals[2–4], direct information concerning brain connections in humans is very limited. Injection of fluorescent dyes *post mortem* allows tracing of tracts, but only for distances of tens of millimeters[5]. Longer-distance connections can be investigated by dissection of major tracts or histological studies of remote degeneration following a focal lesion[6], but such work is based on a relatively small number of informative patients.

A specific, important focus for investigation is the thalamus because nearly all incoming information to the cortex is routed through this deep gray-matter structure. The thalamus is subdivided into cytoarchitectonically distinct nuclei which have different patterns of anatomical connectivity that are well characterized for non-human animals[7,8]. Boundaries between thalamic nuclei that can be visualized histologically[9] are not easily seen in magnetic resonance (MR) images, even using contrast-optimized protoc0ls[10]. If connectivity information were available locally, it could be used as an alternative method for defining boundaries between thalamic subregions and would provide information directly relevant to function.

Diffusion imaging characterizes the apparent diffusion properties of water[11,12]. In tissue with a high degree of directional organization, the diffusion of water protons is different in different directions. In brain white matter, the principal diffusion direction corresponds well with orientation of major fibers in each voxel[13]. Recent developments in diffusion tensor imaging (DTI) techniques have enabled tracing of large fiber tracts in the living human brain[11,14–20]. However, conventional 'streamlining' tract tracing algorithms typically can only progress when there is high certainty of fiber direction (that is, when local diffusion

anisotropy exceeds a specified threshold)[16,19,20]. This has limited their usefulness in defining pathways near gray matter—as they approach their cortical or subcortical targets.

Here, using a probabilistic tractography algorithm, we were able to infer anatomical connectivity that progresses fully into gray matter. We thus provide a comprehensive description of the connections between thalamus and cortex in the human brain *in vivo*. An additional result of this approach is the discrimination of human thalamic subregions on the basis of their connections with the cortex.

RESULTS

We used a fully automated probabilistic tractography algorithm (see Methods) to form connectivity distributions from individual voxels within the thalamus of a single subject. From these distributions, we traced pathways all the way to the cortex (**Fig. 1a–d**). For example, seeding a voxel in the lateral geniculate nucleus (LGN) generated pathways to the visual cortex and optic tract (**Fig. 1a**). The course of generated pathways depends on seed point locations (**Fig. 1b**).

Commonly connected thalamic subregions

We segmented the cortex into large, anatomically defined regions (see Methods) corresponding to known connection areas of the major thalamic nuclear groups in non-human primates (**Fig. 2a**). For every thalamic voxel, the automated tractography algorithm was used to define probability levels for connectivity to each ipsilateral cortical zone. Each thalamic voxel then was classified according to the ipsilateral cortical zone with which it had the highest probability of connectivity. This resulted in clusters of commonly connected voxels within the thalamus. On the basis of the strong correspondence among our connectivity-
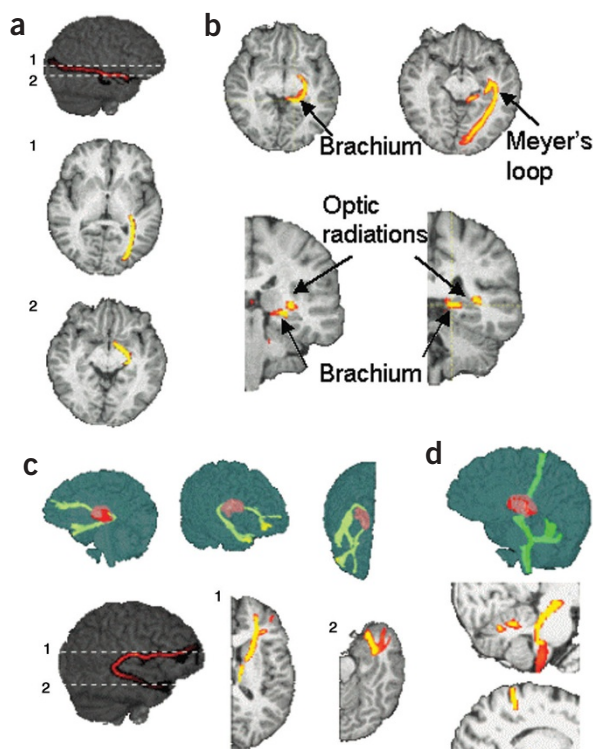
Figure 1 Tracing connectivity distributions from individual seed voxels. Voxels are color-coded according to whether the probability of pathways traveling through that voxel is high (yellow) or low (red). (**a**) From a voxel in putative LGN, the connectivity distribution was traced anteriorly along the optic tract, and posteriorly to the visual cortex, consistent with the well-established anatomy of the visual system. (**b**) Seeding a voxel in the optic tract generated a connectivity distribution such that the multiple pathways generated followed one of two distinct paths. One path went through the LGN and on to visual cortex, corresponding to the optic radiations (as in **a**). A second path corresponded to the brachium of the superior colliculus (axial slice in **b**). The separation of these two paths can be seen in the coronal sections in **b**. The more inferior and medial path follows the brachium and the more superior path follows the optic radiation (as in **a**). Seeding a voxel in the white matter just lateral to the LGN generated a distribution that traveled indirectly to the visual cortex, via the temporal lobe, forming Meyer's loop. The path shown here is a maximum-intensity projection over four axial slices, overlaid on a single slice. (**c**) From a voxel in putative MD, the connectivity distribution progressed anteriorly to the lateral prefrontal cortex and also, at first posteriorly, around the posterior edge of the thalamus, and then anteriorly to the anterior temporal cortex. (**d**) From a voxel in putative VL, the distribution both ascended to the anterior bank of the central sulcus (M1) and descended. The descending distribution followed two distinct paths, one entered the cerebellum and branched, terminating in the cerebellar cortex, and the other continued farther down the brainstem.

based clusters in the human thalamus, known locations of thalamic nuclei in humans[9] and connections in non-human primates[7], we propose that these clusters correspond to different thalamic nuclei or nuclear groups (**Fig. 2**). Note that the description cannot distinguish between thalamocortical and corticothalamic connections, as diffusion-weighted imaging (DWI) is sensitive only to the orientation of fiber tracts and not to their anatomical polarity.

In the monkey, the mediodorsal nucleus (MD) is reciprocally connected to the prefrontal cortex (PFC)[21,22] via the anterior thalamic peduncle and to temporal regions including the temporal pole[23], olfactory cortex[24] and amygdala[25] via the inferior thalamic peduncle. Our results suggest that a similar organization is found in the human brain as a large medial, dorsal region of the thalamus had highly probable prefrontal and temporal connections. We suggest that this region includes MD. Studies in non-human primates have shown that the ventral poste-

rior nucleus (VP) projects to primary and secondary somatosensory areas (S1 and S2)[26]. We found a similar ventral posterior region with a strong probability of somatosensory connections (**Fig. 2c,d**) and suggest this corresponds to the human VP. In monkeys, the ventral lateral (VL) and ventral anterior (VA) nuclei project to primary motor cortex (M1) and premotor cortex (PMC)[27]. A lateral region, anterior to the putative VP, was found to have a high probability of motor cortical connectivity (**Fig. 2c,d**). We suggest that this region includes VL and VA. In the non-human primate, the lateral posterior nucleus (LP) and parts of the pulvinar (Pu) project to posterior parietal cortex (PPC) and extrastriate cortices[7], and medial and inferior parts of the pulvinar are connected to the temporal lobe[28,29]. In the human brain, we found a posterior region that is connected to these areas, and propose that it corresponds to the LP/Pu complex (**Fig. 2c,d**). Confidence in the connectivity parcellations was increased by the finding that the pattern of connections was comparable between left and right thalami.

Nuclear subdivisions

We further divided the cortical surface in the left hemisphere (for example, M1 was separated from PMC; **Fig. 3a**) and re-ran the auto-

Figure 2 Connectivity-based segmentation of the thalamus in a single subject. (**a**) Division of the cerebral cortex according to anatomical landmarks (see Methods). (**b**) An axial section based on a histological atlas of the human thalamus with nuclei outlined by black lines[9]. Nuclei have been color-coded according to the cortical zone to which we predict they would show the strongest connections, on the basis of data from non-human primates[7,21–27]. (**c,d**) Classifying thalamic voxels based on the zone with the highest probability of connection resulted in clusters of commonly-connected voxels. The clusters correspond to histologically defined locations of major nuclei as in **b**. The medial, anterior purple area in **c** and **d** is thought to include the mediodorsal nucleus and nuclei within the anterior complex, which are connected to prefrontal cortex and the temporal lobe. The more posterior purple area is thought to include parts of the lateral and inferior pulvinar which connect to the temporal lobe. The yellow area is thought to include the anterior pulvinar and the lateral posterior nucleus which project mainly to posterior parietal and extrastriate areas. The blue area is thought to include the ventral posterior lateral nucleus, which projects to somatosensory cortices. The orange area is thought to include the ventral lateral and ventral anterior nuclei, which project to motor and premotor cortices.
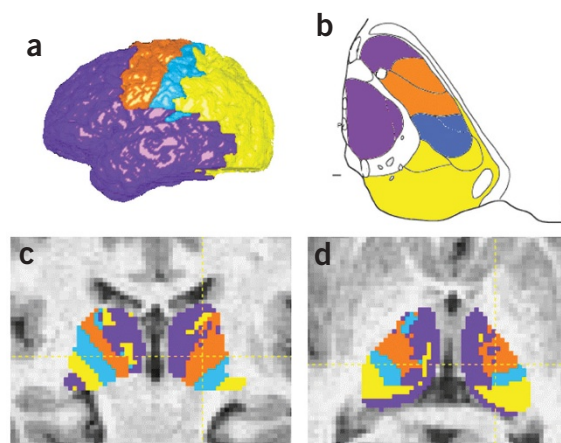
Figure 3 Connectivity-based segmentation of the thalamus. (**a**) Division of the cortex according to anatomical landmarks (see Methods) after cortex. (**b**–**d**) Classification of thalamic voxels based on probable connections to these cortical areas. We propose the following color scheme: anterior, superior and medial purple regions (visible in **c** and **d**) include some of MD, which receives inputs from the temporal lobe, and parts of the anterior complex that project to limbic areas in the medial temporal region; the more posterior and inferior purple region (posterior to the red area, visible in **b** and **d**) includes parts of the medial and inferior pulvinar that project to the temporal lobe; the dark blue region includes some of MD, VA and parts of the anterior complex (AM, AD) that project to the prefrontal cortex; the yellow region includes the anterior parts of the pulvinar that project to PPC; the pale blue area includes LP and VPL, which project to somatosensory cortices; the orange area includes VLp which projects to M1; the green region includes VLa and VA, which project to premotor areas; and the red regions include LGN (visible in coronal section, **c**), parts of the inferior pulvinar (most inferior red areas visible in sagittal section, **d**) and some intralaminar nuclei.
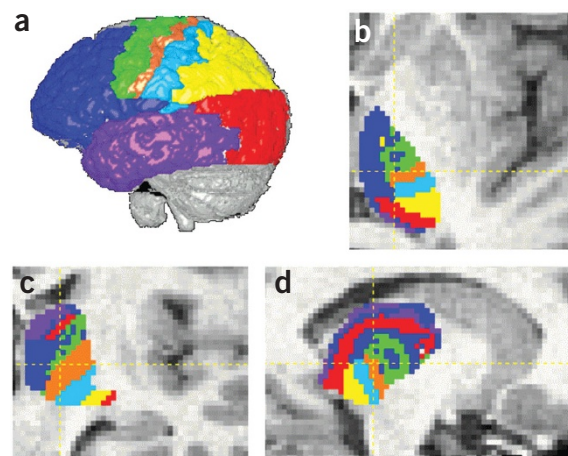
mated tractography-based segmentation for the left thalamus to test for finer thalamic subdivisions. Within the large, lateral clusters, smaller, distinct regions connecting to the somatosensory cortices, M1 and PMC were distributed along a posterior–anterior axis (**Fig. 3b**). From the known anatomy in non-human primates, in which VP projects to somatosensory cortex[26], VLp to area 4 (ref. 30) and VLa and VA to lateral and medial area 6 (ref. 31), we suggest that the clusters we found connected to somatosensory cortices M1 and PMC correspond to VP, VLp and VLa/VA, respectively. On the cortical surface, we also separated PPC from the occipital cortex. We propose that the inferior/lateral area (red in **Fig. 3c**) with the most probable connections to the occipital lobe corresponds to the LGN. The posterior region that connects to PPC (yellow in **Fig. 3**) may include LP and anterior and lateral pulvinar. Medial to this, there are areas that connect to the occipital lobe and to the temporal cortex (red and purple, respectively, in **Fig. 3**). These may include parts of medial and inferior pulvinar, which have been shown to connect to ventral and anterior parts of the temporal lobe in non-human primates[28,29].

Distribution of thalamic pathways within the internal capsule

Thalamocortical pathways are highly organized within the internal capsule[32]. To test the degree to which we could detect this organization, we used the same tractography approach to classify white matter voxels within the internal capsule according to the thalamic region with which they were most strongly connected. The distribution of thalamic pathways within the internal capsule was as expected[32] (**Fig. 4**).

Probabilistic representation of connections

In **Figs. 2** and **3**, classification of thalamic voxels is generated from the highest probability of connectivity to cortical targets. However, information is available on the probability of connectivity to every cortical region for each voxel. Representation of these probabilities demonstrates that some voxels appear connected to more than one cortical region (**Fig. 5**). For example, in the cluster that we propose corresponds to VA, some pathways reached PMC and others reached PFC, consistent with the known distribution of cortical connections of this nucleus in the monkey[21,33] (**Fig. 5**). We also detected PFC connections from the medial pulvinar (**Fig. 5**), again consistent with monkey studies[33].

Paths between thalamus and cortex

Each of the large cortical masks used here includes functionally and anatomically distinct subregions. Information is also available concerning pathway targets within each cortical mask and the path by which they travel to the cortex. We explored this with connections from MD to temporal lobe. A similar approach could be taken with other thalamic subregions and cortical areas.

We generated pathways from all voxels within MD with predominantly temporal lobe connections (**Fig. 6a**) and found that pathways between MD and the temporal lobe take at least two distinct paths (**Fig. 6b**) and terminate in different regions (**Fig. 6b–d**), consistent with data from nonhuman primates[34].

Internal medullary lamina

The classification of thalamic voxels described thus far has been based only on probable connections to cerebral cortex. In monkey thalamus, however, there are thalamic regions with predominantly subcortical connections and only weak or diffuse cortical connections[7]. Similarly, in our data there were regions within the thalamus for which the probability of connection to cortical gray matter was very small. To better define these regions that show lower probabilities of cortical connections, we re-ran analyses with thresholding at various levels (**Fig. 7**). As the threshold was increased, a region between the proposed lateral and medial nuclear groups was defined that did not show suprathreshold connectivity probability to any cortical region (**Fig. 7**). Pathways from this region were generated mainly to the ipsilateral basal ganglia or to contralateral subcortical targets via the corpus callosum. We propose that
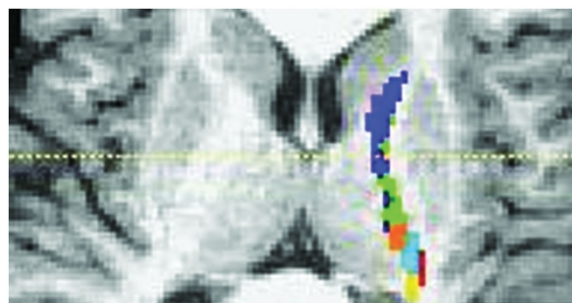

Figure 4 Classification of internal capsule white matter based on connections to putative thalamic nuclei. Voxels are color-coded according to the thalamic region in **Fig. 3** with which they show the strongest connection. The anterior limb of the internal capsule contained probable pathways from putative MD that terminated in the prefrontal cortex. The posterior limb of the internal capsule contained pathways from (in anterior→posterior order) putative VA/VL to premotor cortex, VL to motor cortex, VP to sensory cortices, and pulvinar to temporal and visual cortices.
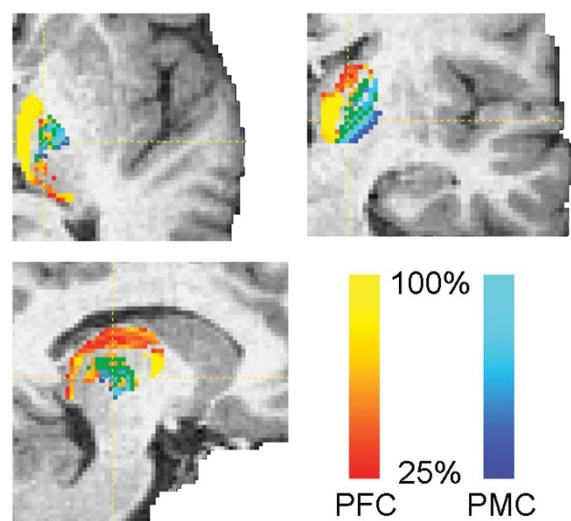
Figure 5 Probabilistic mapping of cortical connections. Regions of overlapping connections are shown in green. Probabilistic mapping of connections to prefrontal cortex (PFC) and premotor cortex (PMC) indicates the presence of a region, which we propose corresponds to the ventral anterior nucleus, with a suprathreshold probability of connections to both regions.

the thalamic region defined in this way includes parts of the internal medullary lamina and the intralaminar nuclei. These nuclei project predominantly to the striatum in the monkey[35], although they also have diffuse cortical connections[7].

Reproducibility between subjects

To explore the reproducibility of the connectivity-based thalamic clusters between subjects, we analyzed data from an additional seven subjects. In five out of seven subjects, the resulting clusters were very similar in location, ordering and size to those in the original subject (**Fig. 8**). In two out of seven subjects, the diffusion data was of poorer quality, and most of the paths generated from certain thalamic regions failed to reach the cortical masks . Even in those two subjects, pathways from the thalamus that did reach cortex had a very similar distribution to those in the original subject. Explicit representation of pathway uncertainty in this approach provides a good criterion to limit false positives.

DISCUSSION

Here we show that it is possible to trace connections from the thalamus to the gray matter of the human cerebral cortex *in vivo* using diffusion imaging. To our knowledge, this is the first report of anatomically specific inferences of connectivity between gray matter structures using diffusion data. This approach should therefore provide new data on human brain connectivity. We found that connections between the thalamus and cortex in humans are largely similar to those previously found

in tracer studies in non-human primates[7,21–31,33–35] and are reproducible across subjects. This similarity to data from non-human primates is apparent not only in the distribution of connections to different cortical sites, but also in the paths that are followed between the thalamus and the cortex.

We also used the probability of connection to different cortical zones as an anatomical classifier for individual thalamic voxels. This generated clusters of voxels showing common patterns of anatomical connectivity to the neocortex. The relative locations and sizes of these clusters corresponded well to histologically defined human thalamic nuclei[9]. The approach used here is generalizable and therefore may be used to map connectivities or anatomically parcel other gray-matter structures. This type of data should complement functional imaging and has the potential to provide new insights into understanding disorders associated with variations in brain structure.

Tracing fibers to cortex has been notoriously difficult when using the maximum-likelihood approaches traditionally used for DTI tractography. As fibers approach cortex, diffusion anisotropy reduces, and calculated principal diffusion directions become increasingly uncertain as a result of image noise (Jones, D.K. *et al. Proc. Intl. Soc. Mag.* **10**, 1122, 2002). This problem is so pronounced that streamlining algorithms used to date have had to apply an arbitrary anisotropy threshold, which forces the early termination of reconstructed pathways[16,19,20]. This has limited attempts to trace pathways directly from deep gray matter, which typically has low anisotropy. In these circumstances, a fully probabilistic algorithm has significant advantages. First, because an explicit representation of uncertainty in path direction is generated, the relative probabilities of directions can be
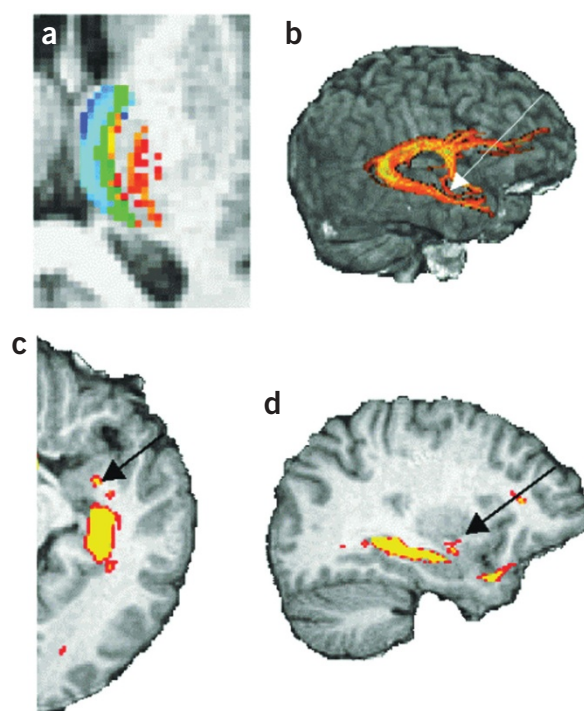
Figure 6 Paths from thalamus to temporal lobe. (**a**) Probabilistic mapping of connections to the temporal (turquoise to blue) and prefrontal (red to yellow) regions or both (green). To investigate the paths and termination sites of connectivity distributions to the temporal cortex, we generated a representation of pathways from all medial voxels with suprathreshold connections to the temporal (and not prefrontal) region (the blue/turquoise area). (**b**) Distributions took two distinct paths to the temporal lobe. The most probable pathway from this region travels around the posterior edge of the thalamus, extends anteriorly through the hippocampal formation, then spreads before terminating in the superior temporal gyrus (temporal pole), the anterior middle temporal gyrus and piriform lobe (as in **Fig. 1c**). A less probable pathway (indicated by arrows in **b**–**d**) extended anteriorly and inferiorly along the medial wall of the thalamus, then turned laterally into the amygdala (**c**,**d**). A similar path, which travels from the amygdala via the inferior thalamic peduncle and enters the anterior head of the thalamus, has been described for non-human primates[34].

Figure 7 Effects of thresholding thalamic clusters based on the probability of connection to cortex. Thresholding at probabilities of 10% (**a,b**), 40% (**c,d**) and 80% (**e,f**). Top, axial images; bottom, coronal images.

estimated, and the pathway can continue even if the probability is low for any single direction. A second useful advantage of a probabilistic algorithm is resistance to noise. It can be difficult to track beyond a noisy voxel using a non-probabilistic algorithm, as it may initiate a meaningless change in path. With a probabilistic algorithm, however, paths that have taken errant routes tend to disperse quickly, so that voxels along these paths are classified with low probability. In contrast, 'true' paths tend to group together, giving a much higher probability of connection for voxels on these paths.

We have used patterns of thalamocortical connectivity inferred from diffusion images to parcel anatomically distinct regions of the thalamus. Although it uses a common imaging technique, this approach is distinct from the differentiation of thalamic regions on the basis of local diffusion properties (Wiegell, M.R. *et al. Proc. Intl. Soc. Mag. Reson.* **8**, 481, 2000; Wiegell, M.R., *et al. Proc. Intl. Mag. Reson.* **7**, 934, 1999) and offers significant advantages as we consider long-distance connectivities. For example, the lateral sensorimotor nuclear group (VLa, VLp, VP) contains voxels that have very similar principal eigenvectors from a diffusion tensor fit, but pathways from the nuclear subdivisions terminate in distinct anatomical regions, allowing their discrimination if connections are followed up to the cortex. Also, by considering not only diffusion measurements within a voxel, but also information available at a more global scale, the thalamic segmentation achieved has a finer spatial resolution than that of the original diffusion images. Together, these characteristics of our approach have allowed us to thoroughly test predictions concerning homologies between human and non-human primate thalamic organization.
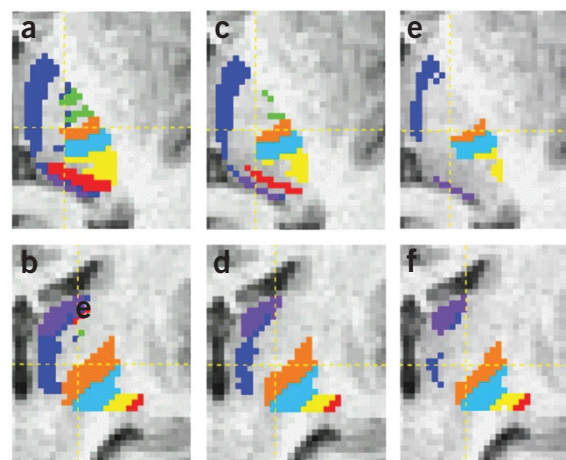
There are limitations to this approach. First, it is impossible to define fiber tract polarity (for example, distinguishing thalamocortical from corticothalamic connections) using diffusion tractography. Second, the method is sensitive primarily to major pathways, and therefore smaller pathways, pathways with sharp path inflections or pathways that cross other tracts are not always detected by our method. For example, from seeds placed within the gray matter of the LGN, we were able to detect the dorsal portion of the optic radiation that travels directly to the visual cortex (**Fig. 1a**). However, detection of the more ventral part of the optic radiation that travels to visual cortex via the temporal cortex (forming Meyer's loop[32]) was possible only from seeds placed in the white matter just lateral to the LGN. Use of higher-resolution imaging and of analysis approaches that explicitly model complex fiber structures within a voxel[36] may increase sensitivity to such paths.

In interpreting the connectivity distributions presented here, it is important to note that our approach does not allow us to infer the true distribution of fiber structure within a voxel, but rather to estimate the uncertainty associated with the principal direction so that we may quantify our confidence in the tractography results. Thus, the distributions that we present are not estimates of true fiber spread from a voxel, but of the confidence bound on the location of the most probable single connection. The width of these confidence bounds will depend both on experimental noise and on any mismatch between our model (a single population of parallel fibers) and the diffusion data (which may reflect complex structure, such as crossing fibers).

Although the patterns that we found correspond well with those defined by direct anatomical studies of non-human primates, further validation of this approach is desirable. For example, cytoarchitectonic boundaries could be defined on the same population imaged, and parallel diffusion and manganese-tracer imaging[37] could test the correspondence between probabilistic tracts and real fiber pathways in non-human primates.
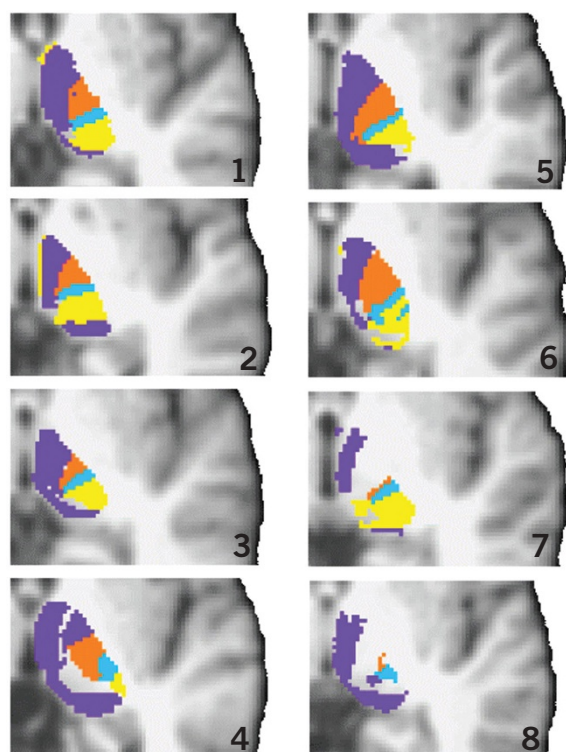

Figure 8 Comparison of connectivity-based segmentation of the thalamus between eight subjects (results from subject 1 are described in greater detail elsewhere in the manuscript). Voxels are color-coded as in **Fig. 2** if at least 1% of generated pathways reached the cortex. Brains have been re-aligned to the same standard brain template and a single axial slice (at Talairach $Z = 0$) is presented. The connectivity-based clusters found in subjects 1–6 were very similar. In subjects 7 and 8, there are some 'gaps' in the thalamus which correspond to regions where fewer than 1% of pathways reached any cortical mask. The patterns in these two subjects are similar to those seen in subject 1 when much higher thresholds were used (see **Fig. 7**).

The current study was limited to the investigation of thalamic connections to large cortical regions. However, the non-human primate literature has provided strong evidence for finer-grained topographic mapping, such as between subregions of MD and smaller regions in the prefrontal cortex[33,38]. Such investigations in the living human brain could proceed as a straightforward extension of the current investigation.

We verified that patterns of anatomical connectivity in the thalamus are reproducible between subjects, but future studies should explore reproducibility quantitatively[15], for example by producing population-level probabilistic maps of connectivity-based clusters, which could be related to cytoarchitectonic and functional maps[39].

There are obvious clinical applications of our methods as well. Probabilistic tractography could help characterize developmental and acquired brain disorders, for example by testing for alterations in fronto-thalamic circuitry in schizophrenia[40] or by defining the relations between quantitative differences in corticocortical connectivity and learning abilities[41]. The ability to define regional boundaries reliably in gray matter could also, for example, be used to more precisely target specific subcortical structures in the treatment of movement disorders by functional neurosurgery[42,43].

METHODS

Data acquisition. Diffusion-weighted data were acquired in eight healthy subjects (6 male, 2 female, ages 26–33, but the majority of the results reported are from a single male subject, aged 33) using echo planar imaging (60 2.3 mm thick slices, f.o.v. = 220 220 mm^2, matrix = 96 96; images were reconstructed on a 128 128 matrix giving a final resolution of 1.7 1.7 2.3 mm^3) implemented on a General Electric 1.5 T Signa Horizon scanner with a standard quadrature head-coil and maximum gradient strength of 22 mT m^{-1}. Informed written consent was obtained from all subjects in accordance with ethical approval from the National Hospital for Neurology and Neurosurgery and Institute of Neurology joint research ethics committee. The diffusion weighting was isotropically distributed[44] along 54 directions (δ = 34 ms, Δ = 40 ms, b-value = 1,150 s mm^{-2}). Six diffusion-weighted volumes (b-value = 300 s mm^{-2}) and six volumes with no diffusion weighting were acquired. The high angular resolution of the diffusion-weighting directions[44] improves the robustness of PDF estimation (see image analysis section below) by increasing the signal-to-noise ratio per unit time and reducing directional bias. Cardiac gating (Wheeler-Kingshott, C.A.M. *et al. Proc. Intl. Soc. Mag. Reson. Med.* **10**, 1118, 2002) was used to minimize artifacts from pulsatile flow of the cerebrospinal fluid. The total scan time for the DWI protocol was approximately (depending on heart rate) 20 min.

The high-resolution T1-weighted scan was obtained with a three-dimensional inversion recovery prepared spoiled gradient echo (IR-SPGR) (f.o.v. = 310 155; matrix = 256 128; in-plane resolution = 1.2 1.2 mm^2; 156 1.2 mm thick slices; TI = 450 ms; TR = 2 s; TE = 53 ms).

Image analysis. Probabilistic diffusion tractography was carried out according to previously proposed methods (Behrens, T.E.J. *et al. Proc. Intl. Soc. Mag. Reson. Med.* **10**, 1160 and 1142, 2002).

Probability distributions of fiber directions at single voxels. Under a voxel-wise model of diffusion (the diffusion tensor (DT) model[12]), it is possible to calculate a maximum likelihood solution for fiber direction within each voxel (the principle eigenvector in the DT case). However, this fiber direction has associated uncertainty, caused both by the potential mix of many fiber directions within a voxel, and by image noise (physiological, thermal and other intrinsic measurement noise)[45]. This uncertainty in the fiber direction may be represented in the form of a probability density function (PDF), which can be expressed as $P(\theta,\phi|\mathbf{Y})$, where (θ,ϕ) is the fiber direction (in spherical polar coordinates) and $\mathbf{Y}$ is the data.

We chose to estimate this distribution using a simple partial volume model, which allows for only one fiber direction, with no fiber spread and an isotropically diffusing compartment within the voxel. The effect of any true fiber divergence within the voxel will thus be seen as greater uncertainty in the principal

fiber direction, as is desirable for probabilistic tractography, rather than as a change of shape in the diffusion profile, as might be the case with a DT model.

The partial volume signal model assumes that the MR measurements are a sum of signal from within a single, homogeneous white-matter tract (which has wholly anisotropic diffusion) and signal from isotropically diffusing free water. So for the ith diffusion weighted acquisition, the predicted signal (μ_i) at each voxel is

$$\mu_i = S_o \left((1-f) \exp(-b_i d) + f \exp(-b_i d \mathbf{r}_i^T \mathbf{RAR}^T \mathbf{r}_i) \right) \tag{1}$$

where S_0 is the MR signal without diffusion weighting, d is the diffusivity, b_i and $\mathbf{r}_i$ respectively are the b-value and gradient direction associated with the ith MR acquisition, f is the volume fraction of anisotropic diffusion in the voxel and $\mathbf{RAR}^T$ is the anisotropic diffusion tensor along the principle diffusion direction (θ,ϕ):

$$A = \begin{bmatrix} 1 & 0 & 0 \\ 0 & 0 & 0 \\ 0 & 0 & 0 \end{bmatrix}$$

and R rotates A such that its principal eigenvector lies along (θ,ϕ).

Note that $\mathbf{r}_i^T\mathbf{RAR}^T\mathbf{r}_i$ may equivalently be written as $\cos^2(\gamma_i)$, where γ_i is the angle between $\mathbf{u}(\theta,\phi)$ (the unit vector along (θ,ϕ)) and $\mathbf{r}_i$, the gradient direction for the ith acquisition. This signal model has parameters $(\theta, \phi, d, S_0, f)$ that must be estimated from the data, and parameters b_i and $\mathbf{r}_i$ that are defined by the acquisition parameters.

The noise is modeled separately for each voxel as i.i.d. (independently identically distributed) Gaussian with a mean of zero and a standard deviation across acquisitions of σ. The probability of seeing the data at each voxel, $\mathbf{Y}$, given the model, M, and any randomly chosen instance (or 'realization') of parameter set, $\Omega = (\theta, \phi, d, S_0, f, \sigma)$, may now be written as:

$$P(\mathbf{Y} | \Omega, M) = \prod_{i=1}^{n} P(y_i | \Omega, M) \tag{2}$$

where

$$P(y_i | \Omega, M) \sim N(\mu_i, \sigma) \tag{3}$$

Using Bayes' equation, we may now write down

$$P(\Omega | \mathbf{Y}, M) = \frac{P(\mathbf{Y} | \Omega, M) P(\Omega | M)}{\int_{\Omega} P(\mathbf{Y} | \Omega, M) P(\Omega | M) d\Omega} \tag{4}$$

where $P(\Omega|\mathbf{Y},M)$ is the joint posterior distribution on the entire parameter set, Ω. $P(\Omega|M)$ are the prior distributions on the model parameters, which are chosen to be noninformative, and therefore have minimal effect on the posterior distribution:

$$P(\theta, \phi) = \frac{\sin(\theta)}{2}, P(d) = P(\sigma^{-2}) = \Gamma(\alpha, \beta), P(f) =$$

$$U(0,1), P(S_o) = U(0, \infty)$$

where $U(0,1)$ is the uniform distribution between 0 and 1, $\Gamma(\alpha,\beta)$ is the incomplete Gamma function (which ensures positivity), and α and β are chosen to give

the prior the highest variance possible within machine precision (making the distribution noninformative).

However, the joint posterior distribution in equation (4) is not the distribution of interest for connectivity estimation. We are interested in the uncertainty in the subset of parameters in Ω that contain directional information (θ,ϕ). The uncertainty in these parameters of interest is contained in the marginal posterior distribution on (θ,ϕ), that is $P(\theta,\phi|Y,M)$ (see, for example, discussions on marginalization[46]):

$$P(\theta, \phi \mid \mathbf{Y}, M) = \int_{\overline{\Omega}} P(\Omega \mid \mathbf{Y}, M) d\,\overline{\Omega} \tag{5}$$

where $\overline{\Omega}$ is the parameter set Ω, excluding (θ,ϕ).

Although the integrals in equations (4) and (5) cannot be solved analytically, Markov Chain Monte Carlo[47] (MCMC) techniques provide a way of drawing samples directly from the marginal distributions of interest at each voxel, implicitly performing the integrals in equations (4) and (5). Specifically, we draw samples from σ^{-2} using a Gibbs sampler[47] and from all other parameters using Metropolis Hastings samplers[47].

Estimating global connectivity. To estimate connectivity from $P(\theta,\phi|Y,M)$ at each voxel, we require a model to take us from these local parameters to parameters describing global connectivity. However, given that we only explicitly model a single fiber direction locally in each voxel, the only global model available to us is a simple binary model. Thus, with knowledge of the parameters (θ,ϕ) at each voxel, we can say that two voxels are connected at a global scale if and only if there is a path between them, through the data (θ,ϕ). Hence we may write:

$$P(\exists A \to B \mid (\theta, \phi)_x) = \begin{cases} 1 \\ \\ 0 \quad otherwise \end{cases} \tag{6}$$

If there is a connecting path through $(\theta,\phi)_x$ where $P(\exists A\to B|(\theta,\phi)_x)$ is the probability of a connecting path between points A and B given a particular realization of $(\theta,\phi)_x$ (note that we use the subscript $\mathbf{x}$ to refer to every voxel in the brain, so $(\theta,\phi)_x$ is the complete set of fiber directions and Y_x is the complete MR data set). However, in the absence of absolute knowledge of $(\theta,\phi)_x$, equation (6) cannot be applied. The PDF of interest instead becomes $P(\exists A\to B|Y_x)$. To calculate this probability of global connectivity, we need to incorporate, for each possible value of fiber direction at every voxel $(\theta,\phi)_x$, the probability of connection given this $(\theta,\phi)_x$, and also the probability of this $(\theta,\phi)_x$ given the acquired MR data. This involves solving the following integrals:

$$P(\exists A \to B \mid \mathbf{Y}_x) =$$

$$\int_0^{2\pi}\int_0^{\pi}\!\!\ldots\!\int_0^{2\pi}\int_0^{\pi} P(\exists A \to B \mid (\theta, \phi)_{local})P((\theta, \phi)_{x_1} \mid \mathbf{Y}_{x_1}) \;\ldots$$

$$P((\theta, \phi)_{x_v} \mid \mathbf{Y}_{x_v})d\theta_{x_1}\,d\phi_{x_1}\;\ldots\;d\theta_{x_v}\,d\phi_{x_v} \tag{7}$$

where $x_1...x_v$ are voxels in the diffusion data.

It can be seen from equation (7) that $P(\exists A\to B|Y_x)$ reduces to $P(\exists A\to B|(\theta,\phi)_x)$ when $P((\theta,\phi)_x|Y_x)$ are delta functions centered on, for example, the principal eigenvector of a diffusion tensor fit. That is, when there is no uncertainty in (θ,ϕ), equation (7) reduces to the streamlining (maximum likelihood) solution (equation 6). However, when local fiber direction is uncertain, $P(\exists A\to B|Y_x)$ will be non-zero for connectivity pathways not on the maximum likelihood streamlines. However, even in the discrete data case, equation (7) represents a $2v$-dimensional (where v is the number of voxels in the brain) integral over distributions with no analytical representation. It therefore has no analytical solution.

Fortunately, as we saw in the previous section, even though explicit integration is not possible, the integral can be computed implicitly by drawing samples from

the resulting distribution. Each sample from $P(\exists A\to B|Y_x)$, in this case, is a streamline through samples from $P((\theta,\phi)_x|Y_x)$.

To generate a single pathway from among all those possible, we choose a single sample (θ,ϕ) from the local distribution at point (x,y,z), then move a distance S (taken to be 0.5 mm) along (θ,ϕ) to a new point (x',y',z'), and continue to follow samples from the local distributions until either the brain surface is reached or the path begins to loop back on itself. This last criterion is implemented by use of a lenient curvature threshold (successive directions must be within 80° of each other) and by testing whether the path passes through the same area more than once.

In summary, the effect of this overall procedure is to incorporate the uncertainty in all local fiber directions, derived from all relevant voxels, to produce the best estimate of the PDF on global connection between two points. Each of the probable pathways generated represents a sample from this global PDF on connectivity.

Pilot investigations showed that distributions based on 10,000 or 100,000 samples did not differ, and so we assumed convergence of each global PDF after 10,000 samples are drawn.

Note that the second part of this method (estimating global connectivity), where we sample from the global PDF on connectivity given knowledge of the local PDFs, has a similar effect to approaches proposed by other groups (see *Proc. Intl. Soc. Mag. Reson. Med.* **10**, 2002; *abstr.* 539 (Lazar, M. & Alexander, A. L.), 1131 (Brun, A. *et al.*) and 1165 (Parker, G.J.M. *et al.*). Crucially, however, here we have estimated the local PDFs from the data, whereas previous work has assumed their form.

Thalamic segmentation. We manually outlined the whole thalamus and a number of cortical zones on the subject's T1-weighted image. For tissue-type segmentation, skull stripping and registration (tools from the Oxford Center for Functional Magnetic Resonance Imaging of the Brain's Software Library, www.fmrib.ox.ac.uk/fsl) were used. We performed probabilistic tissue-type segmentation and partial volume estimation on the T1-weighted image[48]. We thresholded these results to include only voxels estimated at greater than 35% gray matter and used this to mask our cortical regions. We skull-stripped the diffusion-weighted and T1-weighted images[49] and performed affine registration[50] between the first non-diffusion-weighted volume and the T1-weighted image to derive the transformation matrix between the two spaces. From each voxel in the thalamus mask, we drew samples from the connectivity distribution (as above), maintaining knowledge of location in structural and DWI spaces, and recorded the proportion of these samples that passed through each of the cortical masks as the probability of connection to that zone. Hard segmentation was performed by classifying the seed voxel as connecting to the cortical mask with the highest connection probability (**Figs. 2** and **3**). To determine whether voxels showed strong or weak cortical connectivity, we carried out thresholding on the basis of the probability of reaching any cortical mask (**Fig. 7**). Some voxels showed a high probability of connection to more than one cortical mask. To investigate overlapping or branching connections from individual voxels, a probability was assigned for each mask at each voxel, based on the percentage of cortically connected pathways that reach the mask (**Fig. 6**).

Cortical masks. We defined cortical zones that correspond to known thalamic connection sites[7]. First, we defined four exclusive cortical zones using the following landmarks on the T1-weighted image:

Prefrontal/temporal zone: The prefrontal cortex was defined as the lateral and orbital cortex anterior to the inferior and superior precentral sulci, from the dorsal to the orbital brain surface. Medially, this region included the cortex superior to the cingulate sulcus, anterior to the vertical line from the anterior commissure, perpendicular to the plane between the anterior and posterior commissures (VAC) and also the cingulate gyrus, from its anterior edge to the level of the central sulcus. The temporal lobe was defined as the lateral cortex inferior to the lateral fissure, bordered posteriorly by the temporo-occipital incisure where visible, or the anterior occipital sulcus. Medially, the temporal lobe was defined as the cortex anterior to a line from the temporal incisure to the posterior commissure.

Motor zone: This region included M1, supplementary motor area (SMA) and PMC. Laterally, this included cortex anterior to the central sulcus up to and including both banks of the inferior and superior precentral sulci. Medially, this region included cortex anterior to the central sulcus up to the VAC line. Both lateral and medial parts of this region extended from the dorsal surface of the brain

to the level of cingulate sulcus.

Somatosensory zone: This region included S1 and S2. S1 was defined as the posterior bank of central sulcus plus postcentral gyrus, from the dorsal surface of the brain to the lateral fissure. S2 was defined as the superior bank of lateral fissure posterior to the posterior edge of postcentral gyrus.

Parieto-occipital zone: The posterior parietal cortex was defined as the lateral cortex posterior to postcentral gyrus, bordered posteriorly and inferiorly by a line from the posterior-occipital fissure to the lateral fissure. Medially, PPC included regions posterior to the postcentral gyrus, bordered posteriorly by the parietal-occipital fissure and inferiorly by the cingulate gyrus. The occipital lobe was defined as the lateral cortex posterior to anterior occipital sulcus and the temporo-occipital incisure, bordered superiorly by a line from the parietal-occipital fissure to the lateral fissure and the medial cortex inferior to the parietal-occipital fissure and posterior to a line from the temporal incisure to the posterior commissure. The optic tract, where visible, was also included with the occipital lobe in this target mask.

Further analyses were carried out with seven cortical masks. We separated M1 (anterior bank of central sulcus and posterior half of precentral gyrus) from the PMC and SMA (the remainder of the motor zone). We also separated the PPC from the occipital lobe and separated the temporal lobe from the PFC.

The insular cortex was not considered in this analysis.

1. Passingham, R.E., Stephan, K.E. & Kotter, R. The anatomical basis of functional localization in the cortex. *Nat. Rev. Neurosci.* **3**, 606–616 (2002).
2. Barbas, H. & Pandya, D.N. Architecture and frontal cortical connections of the premotor cortex (area 6) in the rhesus monkey. *J. Comp. Neurol.* **256**, 211–228 (1987).
3. Van Essen, D.C., Newsome, W.T., Maunsell, J.H. & Bixby, J.L. The projections from striate cortex (V1) to areas V2 and V3 in the macaque monkey: asymmetries, areal boundaries, and patchy connections. *J. Comp. Neurol.* **244**, 451–480 (1986).
4. Scannell, J.W., Burns, G.A., Hilgetag, C.C., O'Neil, M.A. & Young, M.P. The connectional organization of the corticothalamic system of the cat. *Cereb. Cortex* **9**, 277–299 (1999).
5. Mufson, E.J., Brady, D.R. & Kordower, J.H. Tracing neuronal connections in postmortem human hippocampal complex with the carbocyanine dye DiI. *Neurobiol. Aging* **11**, 649–653 (1990).
6. Van Buren, J.M. & Burke, R.C. Variations and Connections of the Human Thalamus. 1. The Nuclei and Cerebral Connections of the Human Thalamus. (Springer-Verlag, New York, 1972).
7. Jones, E.G. *The Thalamus* (Plenum Press, New York, 1985).
8. Guillery, R.W. & Sherman, S.M. Thalamic relay functions and their role in corticocortical communication: generalizations from the visual system. *Neuron* **33**, 163–175 (2002).
9. Morel, A., Magnin, M. & Jeanmonod, D. Multiarchitectonic and stereotactic atlas of the human thalamus. *J. Comp. Neurol.* **387**, 588–630 (1997).
10. Magnotta, V.A., Gold, S., Andreasen, N.C., Ehrhardt, J.C. & Yuh, W.T. Visualization of subthalamic nuclei with cortex attenuated inversion recovery MR imaging. *Neuroimage* **11**, 341–346 (2000).
11. Basser, P.J., Mattiello, J. & LeBihan, D. MR diffusion tensor spectroscopy and imaging. *Biophys. J.* **66**, 259–267 (1994).
12. Basser, P.J., Mattiello, J. & LeBihan, D. Estimation of the effective self-diffusion tensor from the NMR spin echo. *J. Magn. Reson. B* **103**, 247–254 (1994).
13. Beaulieu, C. & Allen, P.S. Determinants of anisotropic water diffusion in nerves. *Magn. Reson. Med.* **31**, 394–400 (1994).
14. Parker, G.J. *et al.* Initial demonstration of *in vivo* tracing of axonal projections in the macaque brain and comparison with the human brain using diffusion tensor imaging and fast marching tractography. *Neuroimage* **15**, 797–809 (2002).
15. Ciccarelli, O. *et al.* From diffusion tractography to quantitative white matter tract measures: a reproducibility study. *Neuroimage* **18**, 348–359 (2003).
16. Mori, S., Crain, B.J., Chacko, V.P. & van Zijl, P.C. Three-dimensional tracking of

17. Poupon, C. *et al.* Regularization of diffusion-based direction maps for the tracking of brain white matter fascicles. *Neuroimage* **12**, 184–195 (2000).
18. Jones, D.K., Simmons, A., Williams, S.C. & Horsfield, M.A. Non-invasive assessment of axonal fiber connectivity in the human brain via diffusion tensor MRI. *Magn. Reson. Med.* **42**, 37–41 (1999).
19. Conturo, T.E. *et al.* Tracking neuronal fiber pathways in the living human brain. *Proc. Natl. Acad. Sci. USA* **96**, 10422–10427 (1999).
20. Basser, P.J., Pajevic, S., Pierpaoli, C., Duda, J. & Aldroubi, A. *In vivo* fiber tractography using DT-MRI data. *Magn. Reson. Med.* **44**, 625–632 (2000).
21. Tanaka, D. Jr. Thalamic projections of the dorsomedial prefrontal cortex in the rhesus monkey (*Macaca mulatta*). *Brain Res.* **110**, 21–38 (1976).
22. Tobias, T.J. Afferents to prefrontal cortex from the thalamic mediodorsal nucleus in the rhesus monkey. *Brain Res.* **83**, 191–212 (1975).
23. Markowitsch, H.J., Emmans, D., Irle, E., Streicher, M. & Preilowski, B. Cortical and subcortical afferent connections of the primate's temporal pole: a study of rhesus monkeys, squirrel monkeys, and marmosets. *J. Comp. Neurol.* **242**, 425–458 (1985).
24. Yarita, H., Iino, M., Tanabe, T., Kogure, S. & Takagi, S.F. A transthalamic olfactory pathway to orbitofrontal cortex in the monkey. *J. Neurophysiol.* **43**, 69–85 (1980).
25. Russchen, F.T., Amaral, D.G. & Price, J.L. The afferent input to the magnocellular division of the mediodorsal thalamic nucleus in the monkey, Macaca fascicularis. *J. Comp. Neurol.* **256**, 175–210 (1987).
26. Jones, E.G. & Powell, T.P. Connexions of the somatic sensory cortex of the rhesus monkey. *Brain* **93**, 37–56 (1970).
27. Jones, E.G., Wise, S.P. & Coulter, J.D. Differential thalamic relationships of sensory-motor and parietal cortical fields in monkeys. *J. Comp. Neurol.* **183**, 833–881 (1979).
28. Raczkowski, D. & Diamond, I.T. Cortical connections of the pulvinar nucleus in Galago. *J. Comp. Neurol.* **193**, 1–40 (1980).
29. Webster, M.J., Bachevalier, J. & Ungerleider, L.G. Subcortical connections of inferior temporal areas TE and TEO in macaque monkeys. *J. Comp. Neurol.* **335**, 73–91 (1993).
30. Asanuma, C., Thach, W.T. & Jones, E.G. Cytoarchitectonic delineation of the ventral lateral thalamic region in the monkey. *Brain Res.* **286**, 219–235 (1983).
31. Asanuma, C., Thach, W.T. & Jones, E.G. Distribution of cerebellar terminations and their relation to other afferent terminations in the ventral lateral thalamic region of the monkey. *Brain Res.* **286**, 237–265 (1983).
32. Carpenter, M. *Neuroanatomy* (Williams and Wilkins, London, 1978).
33. Goldman-Rakic, P.S. & Porrino, L.J. The primate mediodorsal (MD) nucleus and its projection to the frontal lobe. *J. Comp. Neurol.* **242**, 535–560 (1985).
34. Aggleton, J.P. & Mishkin, M. Projections of the amygdala to the thalamus in the cynomolgus monkey. *J. Comp. Neurol.* **222**, 56–68 (1984).
35. Parent, A., Mackey, A. & De Bellefeuille, L. The subcortical afferents to caudate nucleus and putamen in primate: a fluorescence retrograde double labeling study. *Neuroscience* **10**, 1137–1150 (1983).
36. Tuch, D.S. *et al.* High angular resolution diffusion imaging reveals intravoxel white matter fiber heterogeneity. *Magn. Reson. Med.* **48**, 577–582 (2002).
37. Pautler, R.G., Silva, A.C. & Koretsky, A.P. *In vivo* neuronal tract tracing using manganese-enhanced magnetic resonance imaging. *Magn. Reson. Med.* **40**, 740–748 (1998).
38. Kievit, J. & Kuypers, H.G. Organization of the thalamocortical connexions to the frontal lobe in the rhesus monkey. *Exp. Brain Res.* **29**, 299–322 (1977).
39. Mazziotta, J. *et al.* A probabilistic atlas and reference system for the human brain: International Consortium for Brain Mapping (ICBM). *Philos. Trans. R. Soc. Lond B Biol. Sci.* **356**, 1293–1322 (2001).
40. Andreasen, N.C. *et al.* Schizophrenia and cognitive dysmetria: a positron-emission tomography study of dysfunctional prefrontal-thalamic-cerebellar circuitry. *Proc. Natl. Acad. Sci. USA* **93**, 9985–9990 (1996).
41. Klingberg, T. *et al.* Microstructure of temporoparietal white matter as a basis for reading ability: evidence from diffusion tensor magnetic resonance imaging. *Neuron* **25**, 493–500 (2000).
42. Speelman, J.D., Schuurman, R., De Bie, R.M., Esselink, R.A. & Bosch, D.A. Stereotactic neurosurgery for tremor. *Mov. Disord.* **17** (Suppl. 3), S84–S88 (2002).
43. Pollak, P. *et al.* Treatment results: Parkinson's disease. *Mov. Disord.* **17** (Suppl. 3), S75–S83 (2002).
44. Jones, D.K., Horsfield, M.A. & Simmons, A. Optimal strategies for measuring diffusion in anisotropic systems by magnetic resonance imaging. *Magn Reson. Med.* **42**, 515–525 (1999).
45. Anderson, A.W. Theoretical analysis of the effects of noise on diffusion tensor imaging. *Magn. Reson. Med.* **46**, 1174–1188 (2001).
46. Lee, P.M. *Bayesian Statistics: an Introduction* (Arnold, London, 1997).
47. Gilks, W.R., Richardson, S. & Spiegelhalter, D.J. *Markov Chain Monte Carlo in Practice* (Chapman and Hall/CRC, London, 1996).
48. Zhang, Y., Brady, M. & Smith, S. Segmentation of brain MR images through a hidden Markov random field model and the expectation-maximization algorithm. *IEEE Trans. Med. Imaging* **20**, 45–57 (2001).
49. Smith, S.M. Fast robust automated brain extraction. *Hum. Brain Mapp.* **17**, 143–155 (2002).
50. Jenkinson, M. & Smith, S. Global optimisation for robust affine registration. *Med. Image Anal.* **5**, 143–156 (2001).